10-Qubit Entanglement and Parallel Logic Operations with a Superconducting Circuit

Chao Song,[1,2] Kai Xu,[1,2] Wuxin Liu,[1] Chui-ping Yang,[3] Shi-Biao Zheng,[4,*] Hui Deng,[5] Qiwei Xie,[6]
Keqiang Huang,[5,8] Qiujiang Guo,[1] Libo Zhang,[1] Pengfei Zhang,[1] Da Xu,[1] Dongning Zheng,[5,8]
Xiaobo Zhu,[2,9,†] H. Wang,[1,2,‡] Y.-A. Chen,[2,9] C.-Y. Lu,[2,9] Siyuan Han,[7] and Jian-Wei Pan[2,9]

[1]*Department of Physics, Zhejiang University, Hangzhou, Zhejiang 310027, China*
[2]*CAS Center for Excellence and Synergetic Innovation Center in Quantum Information and Quantum Physics,
University of Science and Technology of China, Hefei, Anhui 230026, China*
[3]*Department of Physics, Hangzhou Normal University, Hangzhou, Zhejiang 310036, China*
[4]*Fujian Key Laboratory of Quantum Information and Quantum Optics,
College of Physics and Information Engineering, Fuzhou University,
Fuzhou, Fujian 350116, China*
[5]*Institute of Physics, Chinese Academy of Sciences, Beijing 100190, China*
[6]*Institute of Automation, Chinese Academy of Sciences, Beijing 100190, China*
[7]*Department of Physics and Astronomy, University of Kansas, Lawrence, Kansas 66045, USA*
[8]*School of Physical Sciences, University of Chinese Academy of Sciences, Beijing 100049, China*
[9]*Shanghai Branch, National Laboratory for Physical Sciences at Microscale and Department of Modern Physics,
University of Science and Technology of China, Shanghai 201315, China*
(Received 12 March 2017; revised manuscript received 4 August 2017; published 3 November 2017)

Here we report on the production and tomography of genuinely entangled Greenberger-Horne-Zeilinger states with up to ten qubits connecting to a bus resonator in a superconducting circuit, where the resonator-mediated qubit-qubit interactions are used to controllably entangle multiple qubits and to operate on different pairs of qubits in parallel. The resulting 10-qubit density matrix is probed by quantum state tomography, with a fidelity of 0.668 ± 0.025. Our results demonstrate the largest entanglement created so far in solid-state architectures and pave the way to large-scale quantum computation.

Entanglement is one of the most counterintuitive features of quantum mechanics. The creation of an increasingly large number of maximally entangled quantum bits (qubits) is central for measurement-based quantum computation [1], quantum error correction [2,3], quantum simulation [4], and foundational studies of nonlocality [5,6] and quantum-to-classical transition [7]. A significant experimental challenge for engineering multiqubit entanglement [8–10] has been noise control [11,12]. With solid-state platforms, the largest number of entangled qubits reported so far is five [10], and further scaling up would be difficult as constrained by the qubit coherence and the employed sequential-gate method.

Superconducting circuits are a promising solid-state platform for quantum state manipulation and quantum computing owing to the microfabrication technology scalability, individual qubit addressability, and ever-increasing qubit coherence time [13]. The past decade has witnessed significant progress in quantum information processing and entanglement engineering with superconducting qubits: the preparation of three- and four-qubit entangled states [14–17], demonstration of elementary quantum algorithms [18,19], realization of three-qubit Toffoli gates, and quantum error correction [20–24]. In particular, a recent experiment has achieved a two-qubit controlled-phase gate with a fidelity above 99% with a superconducting quantum processor [10],

where five transmon qubits with nearest-neighbor coupling are arranged in a linear array. Based on this gate, a five-qubit Greenberger-Horne-Zeilinger (GHZ) state was produced step by step; the number of entangled qubits is increased by one at a time. With a similar architecture consisting of nine qubits, digitized Trotter steps were used to emulate the adiabatic change of the system Hamiltonian that encodes a computational problem [25], where the digital evolution into a GHZ state with a fidelity of 0.55 was demonstrated for a four-qubit system.

In this Letter, we demonstrate a versatile superconducting quantum processor featuring high connectivity with programable qubit-qubit couplings mediated by a bus resonator and experimentally produce GHZ states with up to ten qubits using this quantum processor. The resonator-induced qubit-qubit couplings result in a phase shift that is quadratically proportional to the total qubit excitation number, evolving the participating qubits from an initially product state to the GHZ state after a single collective interaction, irrespective of the number of entangled qubits [26]. We characterize the multipartite entanglement by quantum state tomography achieved by synchronized local manipulations and detections of the entangled qubits and measure a fidelity of 0.668 ± 0.025 for the 10-qubit GHZ state, which confirms the genuine tenpartite entanglement [27] with 6.7 standard deviations (σ). We also implement parallel entangling

operations mediated by the resonator, simultaneously generating three Einstein-Podolsky-Rosen (EPR) pairs; this feature was previously suggested in the context of ion traps [28] and quantum dots coupled to an optical cavity [29], but experimental demonstrations are still lacking.

The superconducting quantum processor is illustrated in Fig. 1(a), which is constructed as ten transmon qubits (Q_j for $j = 1$–10), with resonant frequencies $\omega_j/2\pi$ tunable from 5 to 6 GHz, symmetrically coupled to a central resonator (B), whose resonant frequency is fixed at $\omega_B/2\pi \approx 5.795$ GHz.
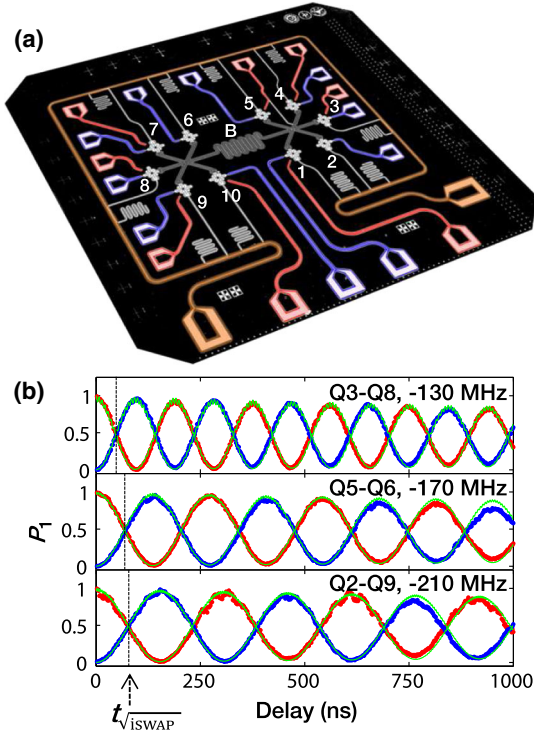

(a)

(b)

FIG. 1. (a) False-color circuit image showing ten superconducting qubits (star shapes) interconnected by a central bus resonator B (gray). Each qubit has its own microwave line (red) for XY control and flux bias line (blue) for Z control, except for Q_2 and Q_6, which share the microwave lines of neighboring qubits. Each qubit has its own readout resonator, which couples to the circumferential transmission line (orange) for simultaneous readout. (b) Parallel intrapair SE interactions for Q_3-Q_8 (top), Q_5-Q_6 (middle), and Q_2-Q_9 (bottom) at the corresponding detunings as indicated. The anticorrelated, time-modulated occupation probabilities P_{10} (red dots) and P_{01} (blue dots) of each pair indicate that energy is exchanged within the pair [6], undisturbed by what happens in the other two pairs: Six qubits in three pairs are measured simultaneously, and we ignore outcomes of the other qubits for the two-qubit data shown in each panel. All directly measured qubit occupation probabilities are corrected for the elimination of the measurement errors [30]. Lines (green) are numerical simulations. The small high-frequency oscillations in the simulation curve (green) for Q_3-Q_8 are due to the relatively small qubit-resonator detuning. These small oscillations can be reduced by using a larger detuning but at the price of a smaller intrapair SE interaction strength.

Measured qubit-resonator (Q_j-B) coupling strengths $g_j/2\pi$ range from 14 to 20 MHz (see Supplemental Material [31] for details on the device, operation, and readout) [43]. The central resonator serves as a multipurpose actuator, enabling controlled long-range logic operations, scalable multiqubit entanglement, and quantum state transfer. In the rotating-wave approximation and ignoring the cross talk between qubits (see Supplemental Material [31]), the Hamiltonian of the system is given by

$$H/\hbar = \omega_B a^+ a + \sum_{j=1}^{10} [\omega_j |1_j\rangle\langle 1_j| + g_j(\sigma_j^+ a + \sigma_j^- a^+)], \quad (1)$$

where σ_j^+ (σ_j^-) is the raising (lowering) operator of Q_j and a^+ (a) is the creation (annihilation) operator of B.

The qubit-qubit coupling can be realized through the superexchange (SE) interaction [44] mediated by the bus resonator B [45–48]. With multiplexing, we can further arrange multiple qubit pairs at different frequencies to turn on the intrapair SE interactions simultaneously. To illustrate this feature, we consider three qubit pairs, Q_k-$Q_{k'}$, Q_l-$Q_{l'}$, and Q_m-$Q_{m'}$, detuned from resonator B by Δ_j ($\equiv \omega_j - \omega_B$, and $\omega_j = \omega_{j'}$) for $j = k$, l, and m, respectively, while all other qubits are far detuned and can be neglected for now. In the dispersive regime and when the resonator B is initially in the ground state, it will remain so throughout the procedure, and the effective Hamiltonian for the qubit pairs is

$$H_1/\hbar = \sum_{j\in\{k,l,m\}} \lambda_j(\sigma_j^- \sigma_{j'}^+ + \sigma_j^+ \sigma_{j'}^-)$$

$$+ \sum_{j\in\{k,l,m\}} \left(\frac{g_j^2}{\Delta_j}|1_j\rangle\langle 1_j| + \frac{g_{j'}^2}{\Delta_j}|1_{j'}\rangle\langle 1_{j'}| \right), \quad (2)$$

where $\lambda_j = (g_j g_{j'}/\Delta_j)$, $|\Delta_j| \gg g_j, g_j'$, and $|\Delta_{j_1} - \Delta_{j_2}| \gg \lambda_{j_1}, \lambda'_{j_1}, \lambda_{j_2}, \lambda'_{j_2}$ for $j_1, j_2 \in \{k, l, m\}$ and $j_1 \neq j_2$. With this setting, the resonator B is simultaneously used for three intrapair SE processes; the interpair couplings are effectively switched off due to large detunings between different pairs.

With the fast Z control on each qubit, coupling between any two qubits can be dynamically turned on and off by matching (intrapair) and detuning (interpair), respectively, their frequencies; i.e., we can reconfigure the coupling structure *in situ* without modifying the physical wiring of the circuit. For example, by arranging Δ_k, Δ_l, and Δ_m in Eq. (2) at three distinct frequencies, we create three qubit pairs (Q_2-Q_9, Q_3-Q_8, and Q_5-Q_6) featuring programable intrapair SE interactions with negligible interpair cross talk, enabling parallel couplings as demonstrated in Fig. 1(b). According to the probability evolutions shown in Fig. 1(b), a characteristic gate time $t_{\sqrt{\mathrm{iSWAP}}}$ for each qubit pair can be identified.

Operating multiple pairs in parallel naturally produces multiple EPR pairs [45,46]. As the pulse sequence shows in Fig. 2(a), three EPR pairs are produced after the completion
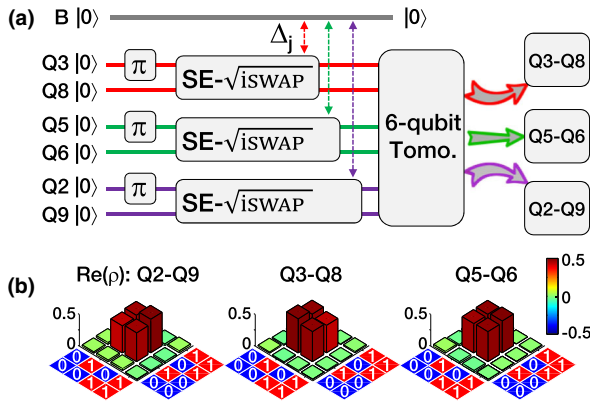
FIG. 2. (a) Pulse sequence with detunings listed in Fig. 1(b). Tomography is performed to reconstruct the six-qubit density matrix, over which we perform partial trace to obtain the reduced density matrix of each EPR pair. Each π-rotation (tomographic $\pi/2$-rotation) pulse has a length of 60 (30) ns and a full width half maximum of 30 (15) ns, designed following the derivative reduction by adiabatic gate (DRAG) control theory [49]. (b) Real parts of the reconstructed two-qubit density matrices for the three EPR pairs of Q_2-Q_9, Q_3-Q_8, and Q_5-Q_6, with fidelities (concurrences) of 0.932 ± 0.13 (0.869 ± 0.026), 0.957 ± 0.010 (0.915 ± 0.019), and 0.951 ± 0.010 (0.909 ± 0.019), respectively. For clarity of display, single-qubit z-axis rotations are numerically applied to Q_2 (93°), Q_3 (165°), and Q_5 (42°) to cancel the arguments of the major off-diagonal elements.

of all three SE-$\sqrt{\text{iSWAP}}$ gates [48], with the six-qubit quantum state tomography measuring an overall state fidelity of 0.904 ± 0.018. The inferred density matrix ρ is validated by satisfying the physical constraints of Hermitian, unit trace, and positive semidefinite. We further perform partial trace on ρ to obtain three two-qubit reduced density matrices, each corresponding to a EPR pair with a fidelity above 0.93 [Fig. 2(b)].

Remarkably, our architecture allows the high-efficiency generation of multiqubit GHZ states. In contrast to the previous approach where GHZ states are generated by a series of controlled-NOT (CNOT) gates [10], here all the qubits connected to the bus resonator can be entangled with a single collective qubit-resonator interaction. In the theoretical proposal [26,50], N qubits are assumed to be equally coupled to the resonator and are detuned from the resonator by the same amount Δ that is much larger than the qubit-resonator coupling. When all qubits are initialized in the same equal superpositions of $0\rangle$ and $|1\rangle$, e.g., $(|0\rangle - i|1\rangle)/\sqrt{2}$, the SE interaction does not induce any energy exchange between qubits; instead, it produces a dynamic phase that nonlinearly depends upon the collective qubit excitation number k as $k(N+1-k)\theta$, where θ is determined by the effective qubit-qubit coupling strength and the interaction time. With the choice $\theta = \pi/2$, this gives rise to the GHZ state $(|+_1, +_2, ..., +_N\rangle + i|-_1, -_2, ..., -_N\rangle)/\sqrt{2}$, where $|\pm\rangle = (|0_j\rangle \pm i^N|1_j\rangle)/\sqrt{2}$ [26].

Here we apply this proposal to our experiment. We find that, though the qubit-resonator couplings are not uniform and unwanted cross talk couplings exist in our circuit, we can optimize each qubit's detuning and the overall interaction time to achieve GHZ states with high fidelities as guided by the numerical simulation. The pulse sequence is shown in Fig. 3(a). We start with initializing the chosen N qubits in $(|0\rangle - i|1\rangle)/\sqrt{2}$ by applying $\pi/2$ pulses at their respective idle frequencies, following which we bias them to nearby $\Delta/2\pi \approx -140$ MHz for an optimized duration of approximately twice $t_{\sqrt{\text{iSWAP}}}$. The phase of each qubit's XY drive is calibrated according to the rotating frame with respect to Δ, ensuring that all N qubits are in the same initial state just before their SE interactions are switched on [16,31]. After the optimized interaction time, these qubits approximately evolve to the GHZ state $|\Psi_1\rangle = (|+_1, +_2, ..., +_N\rangle + e^{i\varphi}|-_1, -_2, ..., -_N\rangle)/\sqrt{2}$, where φ may not be equal to $\pi/2$ as in the ideal case with uniform qubit-qubit interactions; however, this phase variation does not affect entanglement. Later on, we bias these N qubits back to their idle frequencies; during the process, a dynamical phase ϕ_j is accumulated between $|0\rangle$ and $|1\rangle$ of Q_j. Redefining $|\pm_j\rangle = (|0_j\rangle \pm i^N e^{i\phi_j}|1_j\rangle)/\sqrt{2}$ ensures that the above-mentioned formulation of $|\Psi_1\rangle$ remains invariant, which is equivalent to a z-axis rotation of the x-y-z reference frame, i.e., $x \rightarrow x'$ and $y \rightarrow y'$. Tracking the new axes is important for characterization of the produced GHZ states.

Tomography of the produced states requires individually measuring the qubits in bases formed by the eigenvectors of the Pauli operators X, Y, and Z, respectively. Measurement in the Z basis can be directly performed. For each state preparation and measurement event, we record the 0 or 1 outcomes of each qubit and do so for N qubits simultaneously; repeating the state preparation and measurement event thousands of times, we count 2^N probabilities of $\{P_{00...0}, P_{00...1}, ..., P_{11...1}\}$. Measurement in the X (Y) basis is achieved by inserting a Pauli Y (X) rotation on each qubit before readout. All directly measured qubit occupation probabilities are corrected for elimination of the measurement errors [30]. The 3^N tomographic operations and the 2^N probabilities for each operation allow us to reconstruct all elements of the density matrix ρ (see Supplemental Material [31] for various aspects of our tomography technique including measurement stability, reliability with a reduced sampling size, and preprocessing for minimizing the computational cost). The resulting 10-qubit GHZ density matrix is partially illustrated in Fig. 3(b), with a fidelity of 0.668 ± 0.025, and the N-qubit GHZ fidelity as a function of N is plotted in Fig. 3(b), inset. The achieved fidelities are well above the threshold for genuine multipartite entanglement [27].

The full tomography technique, though general and accurate, is costly when N is large. The produced GHZ
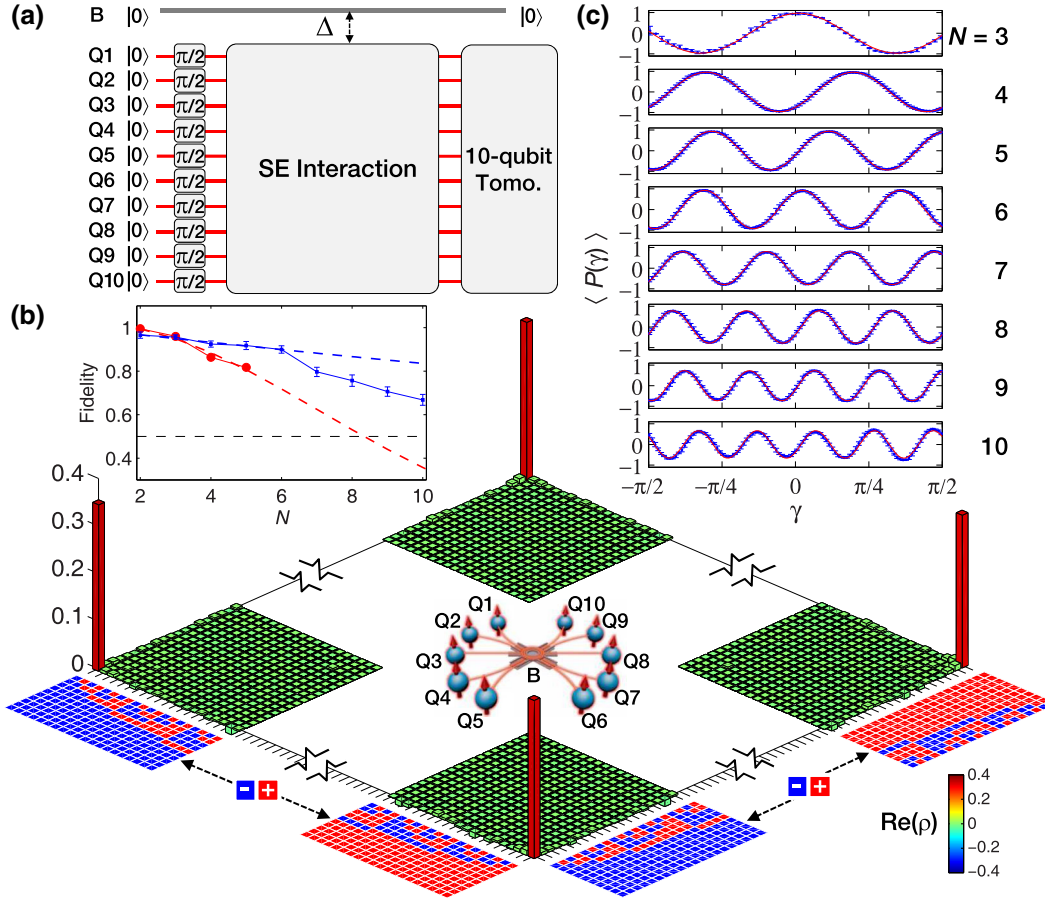
FIG. 3. (a) Pulse sequence for the 10-qubit GHZ state with $\Delta/2\pi \approx -140$ MHz. (b) Partial elements of the measured 10-qubit density matrix, with a fidelity of $\mathrm{tr}(\rho_{\mathrm{ideal}}\rho_{\mathrm{exp}}) = 0.668 \pm 0.025$ relative to the ideal GHZ state $|\Psi_1\rangle = (|+_1, +_2, ..., +_N\rangle + e^{i\varphi}|-_1, -_2, ..., -_N\rangle)/\sqrt{2}$. For clarity of display, here a single-qubit rotation around the x' axis by an angle of φ is numerically applied to one of the qubits, which cancels the arguments of the dominant off-diagonal elements. Center inset: Cartoon illustration showing ten entangled qubits. Top-left inset: Experimentally measured GHZ fidelity (blue dots) and the data adapted from Ref. [10] (red dots) as functions of the qubit number N. Error bars are 1σ. Blue and red dashed lines are guides of different error trends. (c) Parity oscillations observed for the N-qubit GHZ states $|\Psi_2\rangle$ defined as superpositions of the basis states $|0_1, 0_2, ..., 0_N\rangle$ and $|1_1, 1_2, ..., 1_N\rangle$ with $N = 3$–10. The fringe amplitudes are 0.964 ± 0.016, 0.956 ± 0.018, 0.935 ± 0.020, 0.926 ± 0.026, 0.796 ± 0.023, 0.782 ± 0.025, 0.729 ± 0.028, and 0.660 ± 0.032 from top to bottom. For $N = 10$, the state preparation and measurement sequence is repeated 81 000 times for a sample size large enough to count the 2^N probabilities.

states can also be characterized by a shortcut, since the ideal GHZ density matrix consists of only four nonzero elements in a suitably chosen basis. To do so, we apply to each qubit a $\pi/2$ rotation around its y' or x' axis, transforming $|\Psi_1\rangle$ to $|\Psi_2\rangle = (|00...0\rangle + e^{i\varphi}|11...1\rangle)/\sqrt{2}$ (here and below, we omit the subscripts of the qubit index for clarity). The diagonal elements $\rho_{00...0}$ and $\rho_{11...1}$ can be directly measured; the off-diagonal elements $\rho_{00...0,11...1}$ and $\rho_{11...1,00...0}$ can be obtained by measuring the system parity, defined as the expectation value of the operator $P(\gamma) = \otimes_{j=1}^{N}(\cos\gamma Y_j' + \sin\gamma X_j')$, which is given by $\langle P(\gamma)\rangle = 2|\rho_{00...0,11...1}|\cos(N\gamma + \varphi)$ for $|\Psi_2\rangle$ [9]. Polarization along the axis defined by $\cos\gamma Y' + \sin\gamma X'$ can be measured after applying to each qubit a rotation by an angle γ around the z' axis [16]. The oscillation patterns of the measured parity as

functions of γ confirm the existence of coherence between the states $|00...0\rangle$ and $|11...1\rangle$ [Fig. 3(c)]. The fidelity of the N-qubit GHZ state $|\Psi_2\rangle$ can be estimated using the four nonzero elements, which is 0.660 ± 0.020 for $N = 10$. This value agrees with that of the GHZ state $|\Psi_1\rangle$ obtained by full state tomography.

A key advantage of the present protocol for generating GHZ states is its high scalability as demonstrated in Fig. 3(b). If limited by decoherence, the achieved fidelity based on the sequential-CNOT approach, $F_{N,C}$, scales approximately as $F_{N,C} \propto F_{2,C}^{N^2/2}$ at large N [see the red dashed line in Fig. 3(b), inset], while that based on our protocol scales as $F_N \propto F_2^N$ (blue dashed line). Here $F_{2,C}$ (F_2) is quoted as the decoherence-limited fidelity of the CNOT gate (present protocol) involving two qubits. The

falling of the experimental data (blue dots) below the scaling line when $N \geq 6$ is due to the inhomogeneity of g_j and the cross talk couplings. One can see that, even with the two-qubit gate fidelity above 0.99 as demonstrated in two recent experiments [10,51], the coherence performance of the devices does not allow the generation of a 10-qubit GHZ state with fidelity above the genuine entanglement threshold using the sequential-CNOT approach.

In summary, our experiment demonstrates the viability of the multiqubit-resonator-bus architecture with essential functions including high-efficiency entanglement generation and parallel logic operations. We deterministically generate the 10-qubit GHZ state, the largest multiqubit entanglement ever created in solid-state systems, which is verified by quantum state tomography for the first time as well. In addition, our approach allows instant *in situ* rewiring of the qubits, featuring all-to-all connectivity that is critical in a recent proposal [52]. These unique features show the great potential of the demonstrated approach for scalable quantum information processing.

C. S. and K. X. contributed equally to this work.

---

*t96034@fzu.edu.cn
†xbzhu16@ustc.edu.cn
‡hhwang@zju.edu.cn

[1] R. Raussendorf and H. J. Briegel, Phys. Rev. Lett. **86**, 5188 (2001).
[2] A. R. Calderbank and P. W. Shor, Phys. Rev. A **54**, 1098 (1996).
[3] E. Knill, Nature (London) **434**, 39 (2005).
[4] S. Lloyd, Science **273**, 1073 (1996).
[5] D. M. Greenberger, M. A. Horne, A. Shimony, and A. Zeilinger, Am. J. Phys. **58**, 1131 (1990).
[6] M. Ansmann et al., Nature (London) **461**, 504 (2009).
[7] A. J. Leggett, Rep. Prog. Phys. **71**, 022001 (2008).
[8] X. L. Wang et al., Phys. Rev. Lett. **117**, 210502 (2016).
[9] T. Monz, P. Schindler, J. T. Barreiro, M. Chwalla, D. Nigg, W. A. Coish, M. Harlander, W. Hansel, M. Hennrich, and R. Blatt, Phys. Rev. Lett. **106**, 130506 (2011).
[10] R. Barends et al., Nature (London) **508**, 500 (2014).
[11] L. F. Wei, Y. X. Liu, and F. Nori, Phys. Rev. Lett. **96**, 246803 (2006).
[12] S. Matsuo, S. Ashhab, T. Fujii, F. Nori, K. Nagai, and N. Hatakenaka, in *Quantum Communication, Measurement and Computing*, edited by O. Hirota, J. H. Shapiro, and M. Sasaki (National Institute of Information and Communications Technology Press, Tokyo, 2006), No. 8.
[13] J. Q. You and F. Nori, Nature (London) **474**, 589 (2011).
[14] L. DiCarlo, M. D. Reed, L. Sun, B. R. Johnson, J. M. Chow, J. M. Gambetta, L. Frunzio, S. M. Girvin, M. H. Devoret, and R. J. Schoelkopf, Nature (London) **467**, 574 (2010).
[15] M. Neeley et al., Nature (London) **467**, 570 (2010).
[16] Y. P. Zhong et al., Phys. Rev. Lett. **117**, 110501 (2016).
[17] H. Paik et al., Phys. Rev. Lett. **117**, 250502 (2016).
[18] L. DiCarlo et al., Nature (London) **460**, 240 (2009).
[19] M. Mariantoni et al., Science **334**, 61 (2011).
[20] A. Fedorov, L. Steffen, M. Baur, and A. Wallraff, Nature (London) **481**, 170 (2012).
[21] M. Takita, A. D. Córcoles, E. Magesan, B. Abdo, M. Brink, A. Cross, J. M. Chow, and J. M. Gambetta, Phys. Rev. Lett. **117**, 210505 (2016).
[22] D. Ristè, S. Poletto, M.-Z. Huang, A. Bruno, V. Vesterinen, O.-P. Saira, and L. DiCarlo, Nat. Commun. **6**, 6983 (2015).
[23] D. Ristè, M. Dukalski, C. A. Watson, G. de Lange, M. J. Tiggelman, Ya. M. Blanter, K. W. Lehnert, R. N. Schouten, and L. DiCarlo, Nature (London) **502**, 350 (2013).
[24] M. D. Reed, L. DiCarlo, S. E. Nigg, L. Sun, L. Frunzio, S. M. Girvin, and R. J. Schoelkopf, Nature (London) **482**, 382 (2012).
[25] R. Barends et al., Nature (London) **534**, 222 (2016).
[26] S. B. Zheng, Phys. Rev. Lett. **87**, 230404 (2001).
[27] O. Gühne and G. Tóth, Phys. Rep. **474**, 1 (2009).
[28] A. Sørensen and K. Mølmer, Phys. Rev. Lett. **82**, 1971 (1999).
[29] A. Imamoglu, D. D. Awschalom, G. Burkard, D. P. DiVincenzo, D. Loss, M. Sherwin, and A. Small, Phys. Rev. Lett. **83**, 4204 (1999).
[30] Y. Zheng et al., Phys. Rev. Lett. **118**, 210504 (2017).
[31] See Supplemental Material at http://link.aps.org/supplemental/10.1103/PhysRevLett.119.180511 for more information on the device performance and the tomography experiment, which includes Refs. [32–42].
[32] C. Song et al., Nat. Commun. **8**, 1061 (2017).
[33] J. E. Johnson, C. Macklin, D. H. Slichter, R. Vijay, E. B. Weingarten, John Clarke, and I. Siddiqi, Phys. Rev. Lett. **109**, 050506 (2012).
[34] D. Risté, J. G. van Leeuwen, H.-S. Ku, K. W. Lehnert, and L. DiCarlo, Phys. Rev. Lett. **109**, 050507 (2012).
[35] Z. Chen et al. Phys. Rev. Lett. **116**, 020501 (2016).
[36] X. Y. Jin et al. Phys. Rev. Lett. **114**, 240501 (2015).
[37] J. M. Chow et al., Phys. Rev. Lett. **107**, 080502 (2011).
[38] J. Kelly et al., Phys. Rev. Lett. **112**, 240504 (2014).
[39] M. Hofheinz et al., Nature (London) **459**, 546 (2009).
[40] E. Jeffrey et al., Phys. Rev. Lett. **112**, 190504 (2014).
[41] D. Vion (private communication).
[42] H. Wang et al., Phys. Rev. Lett. **106**, 060401 (2011).
[43] E. Lucero et al., Nat. Phys. **8**, 719 (2012).
[44] S. Trotzky, P. Cheinet, S. Fölling, M. Feld, U. Schnorrberger, A. M. Rey, A. Polkovnikov, E. A. Demler, M. D. Lukin, and I. Bloch, Science **319**, 295 (2008).
[45] S. B. Zheng and G. C. Guo, Phys. Rev. Lett. **85**, 2392 (2000).

PHYSICAL REVIEW LETTERS

[46] S. Osnaghi, P. Bertet, A. Auffeves, P. Maioli, M. Brune, J. M. Raimond, and S. Haroche, Phys. Rev. Lett. **87,** 037902 (2001).

[47] J. Majer *et al.*, Nature (London) **449,** 443 (2007).

[48] A. Dewes, F. R. Ong, V. Schmitt, R. Lauro, N. Boulant, P. Bertet, D. Vion, and D. Esteve, Phys. Rev. Lett. **108,** 057002 (2012).

[49] F. Motzoi, J. M. Gambetta, P. Rebentrost, and F. K. Wilhelm, Phys. Rev. Lett. **103,** 110501 (2009).

[50] G. S. Agarwal, R. R. Puri, and R. P. Singh, Phys. Rev. A **56,** 2249 (1997).

[51] S. Sheldon, E. Magesan, J. M. Chow, and J. M. Gambetta, Phys. Rev. A **93,** 060302(R) (2016).

[52] Y. Li and S. C. Benjamin, arXiv:1702.05657.